Brewster's angle silicon wafer terahertz linear polarizer

Antoine Wojdyla, Guilhem Gallot

Brewster's angle silicon wafer terahertz linear polarizer

Antoine Wojdyla and Guilhem Gallot*

Laboratoire d'Optique et Biosciences, École Polytechnique, CNRS, 91128 Palaiseau, France
INSERM U696, 91128 Palaiseau, France
*guilhem.gallot@polytechnique.edu

Abstract: We present a new cost-effective terahertz linear polarizer made from a stack of silicon wafers at Brewster's angle, andevaluate its performances. We show that this polarizer is wide-band, has a high extinction ratio ($> 6 \times 10^3$) and very small insertion losses ($< 1\%$). We provide measurements of the temporal waveforms after linearly polarizing the THz beam and show that there is no distortion of the pulse. We compare its performances with a commercial wire-grid polarizer, and show that the Brewster's angle polarizer can conveniently be used to control the power of a terahertz beam.

OCIS codes: (300.6495) Spectroscopy, terahertz; (260.5430) Polarization.

References and links

1. D. Grischkowsky, S. R. Keiding, M. van Exter, and C. Fattinger, "Far-infrared time-domain spectroscopy with terahertz beams of dielectrics and semiconductors," J. Opt. Soc. Am. B **7**, 2006–2015 (1990).
2. Q. Wu and X. C. Zhang, "Ultrafast electro-optic field sensors," Appl. Phys. Lett. **68**(12), 1604–1606 (1996).
3. D. Mittleman, *Sensing with Terahertz Radiation* (Springer, 2003).
4. C.-F. Hsieh, Y.-C. Lai, R.-P. Pan, and C.-L. Pan, "Polarizing terahertz waves with nematic liquid crystals," Opt. Lett. **33**(11), 1174–1176 (2008).
5. I. Yamada, K. Takano, M. Hangyo, M. Saito, and W. Watanabe, "Terahertz wire-grid polarizers with micrometer-pitch Al gratings," Opt. Lett. **34**(3), 274–276 (2009).
6. H. Dong, Y. Gong, V. Paulose, and M. Hong, "Polarization state and Mueller matrix measurements in terahertz-time domain spectroscopy," Opt. Commun. **282**, 3671–3675 (2009).
7. J.-B. Masson and G. Gallot, "Terahertz achromatic quarter-wave plate," Opt. Lett. **31**(2), 265–267 (2006).
8. A. E. Costley, K. H. Hursey, G. F. Neill, and J. M. Ward, "Free-standing fine-wire grids; their manufacture, performance, and use at millimeter and submillimeter wavelengths," J. Opt. Soc. Am. **67**(7), 979–981 (1977).
9. T. Kondo, T. Nagashima, and M. Hangyo, "Fabrication of wire-grid-type polarizers for THz region using a general-purpose color printer," Jpn. J. Appl. Phys. **42**, L373–L375 (2003).
10. L. Sun, Z.-H. Lv, W. Wu, W.-T. Liu, and J.-M. Yuan, "Double-grating polarizer for terahertz radiation with high extinction ratio," Appl. Opt. **49**, 2066-2071 (2010).
11. S. K. Awasthi, A. Srivastava, U. Malaviya, and S. P. Ojha, "Wide-angle, broadband plate polarizer in Terahertz frequency region," Solid State Commun. **148**, 506–509 (2008).
12. I. Yamada, K. Takano, M. Hangyo, M. Saito, and W. Watanabe, "Terahertz wire-grid polarizer with micrometer-pitch Al gratings," Opt. Lett. **34**, 274–276 (2009).
13. L. Ren, C. Pint, L. Booshehri, W. Rice, X. Wang, D. Hilton, K. Takeya, I. Kawayama, M. Tonouchi, R. Hauge, and J. Kono, "Carbon nanotube terahertz polarizer," Nano Lett. **9**, 2610-2613 (2009).
14. J.-S. Li, D.-G. Xu, and J.-Q. Yao, "Compact terahertz wave polarizing beam splitter," Appl. Opt. **49**(24), 4494–4497 (2010).
15. J.-B. Masson, M.-P. Sauviat, J.-L. Martin, and G. Gallot, "Ionic contrast terahertz near field imaging of axonal water fluxes," Proc. Natl. Acad. Sci. U.S.A. **103**(13), 4808–4812 (2006).
16. R. mendis and D. Mittleman, "A 2-D artificial dielectric with $0 \leq n < 1$ for the terahertz region," IEEE Trans. Microwave Theory Tech. **58**(7), 1993–1998 (2010).
17. A. V. Spivey and S. Cundiff, "Brewster's angle attenuator for terahertz pulses," Appl. Opt. **41**, 2408–2412 (2002).

#146467 - $15.00 USD Received 26 Apr 2011; revised 17 Jun 2011; accepted 18 Jun 2011; published 8 Jul 2011

18. G. L. Carr, M. C. Martin, W. R. McKinney, K. Jordan, G. R. Neil, and G. P. Williams, "High-power terahertz radiation from relativistic electrons," Nature **420**, 153–156 (2002).
19. M. Born and E. Wolf, *Principle of Optics*, 7th Ed. (Cambridge University Press, 1999).
20. D. Brewster, *A Treatise on Optics* (MacMillan and Co., 1831).
21. E. Hecht, *Optics*, 2nd ed. (Addison-Wesley, 1990).

1. Introduction

The Terahertz (THz) band of the electromagnetic spectrum experienced major breakthroughs in the past two decades, thanks to the availability of ultrafast femtosecond lasers, and the development of down-conversion elements such as photo-switch antennas or optical rectification devices, which allow the production of single-cycle THz pulses [1, 2]. Much interest has been applied to characterizing and manipulating the THz beams, but polarization handling is still challenging, in particular due to the inherent broadband spectrum of the single-cycle THz pulses [3]. The key elements of polarization control are polarizers and wave-plates and many improvements emerged in recent years [4–7].

As terahertz polarizers, wire-grid polarizers adapted from microwave technology are readily available [8] and can even be made by using a general-purpose printer [9], but they are not inherently achromatic, and suffer from non-negligible losses. Glan-type polarizers are very difficult to design in the terahertz range due to the lack of transparent birefringent crystals. Other polarizers with good performance have been designed, such as double-grating polarizers [10], layered media [11], wire-grid with Al gratings [12], carbon nanotubes [13] or polarizing beam splitters [14]. However, they experience Fabry-Pérot-like echoes at interfaces, which alter the shape of the THz pulses and are troublesome in time-domain imaging techniques [15]. Brewster's effect in the terahertz region has also been investigated in parallel-plate waveguides [16].

We present a new linear polarizer working in the THz range, based on a silicon wafer stack arranged at Brewster's angle, building a Brewster's Polarizer (BP). Inexpensive industry-grade silicon wafers have quasi-constant refractive index of 3.41 and relatively low absorption coefficient that can be neglected due to the thinness of the wafers [1].

Our experiment provides a textbook example of what is happening inside such a Brewster polarizer. Moreover, the fine control of the polarization gives the ability to precisely modulate the power of the THz beam, an interesting feature when it comes to analyzing the linearity of THz setups [17] or using non-linear effects [18].

2. Theoretical background

The Fresnel coefficients for transmission and reflection in amplitude for both transverse electric (s-) and transverse magnetic (p-) polarizations at the interface between air and plate, are given by [19] under an incidence angle θ_1 (see Fig. 1):

$$t_{12}^s(\theta_1,\theta_2) = \frac{2\cos\theta_1\sin\theta_2}{\sin(\theta_1+\theta_2)} \qquad r_{12}^s(\theta_1,\theta_2) = -\frac{\sin(\theta_1-\theta_2)}{\sin(\theta_1+\theta_2)} \tag{1}$$

$$t_{12}^p(\theta_1,\theta_2) = \frac{2\cos\theta_1\sin\theta_2}{\sin(\theta_1+\theta_2)\cos(\theta_1-\theta_2)} \qquad r_{12}^p(\theta_1,\theta_2) = \frac{\tan(\theta_1-\theta_2)}{\tan(\theta_1+\theta_2)} \tag{2}$$

where θ_2 is the refracted angle given by Snell-Descartes law as $\sin\theta_1 = n\sin\theta_2$ and n is the refractive index of the plate. Therefore, the total amplitude transmissions through the plate of thickness e, taking into account Fabry-Pérot effects, are easily calculated, for both s- and

#146467 - $15.00 USD Received 26 Apr 2011; revised 17 Jun 2011; accepted 18 Jun 2011; published 8 Jul 2011

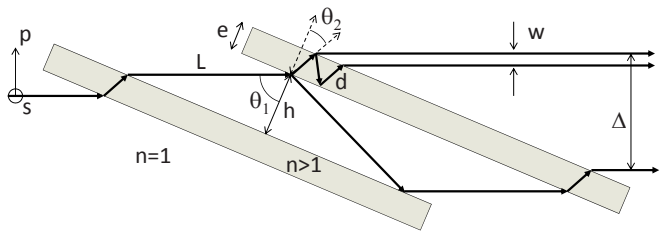

Fig. 1. Schematic of the transmission through parallel plates, for s- and p-polarizations.

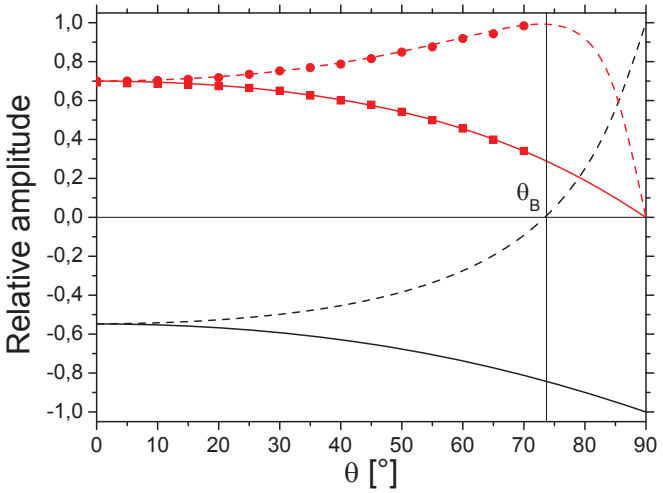

Fig. 2. Fresnel reflection coefficients for a single air-silicon interface (black) and transmission coefficients through a full silicon wafer (red), both for s- (solid) and p-polarization (dashed). The lines are theoretical calculations, and the dots are the corresponding experimental terahertz measurements.

p-polarizations, as

$$T = n\frac{t_{12}(\theta_1,\theta_2)t_{21}(\theta_2,\theta_1)\,e^{i\beta}\,e^{-i\alpha}}{1+r_{12}(\theta_1,\theta_2)r_{21}(\theta_2,\theta_1)e^{2i\beta}} \quad \text{with} \quad \begin{cases} \alpha = \dfrac{2\pi}{\lambda}\dfrac{\cos(\theta_1-\theta_2)}{\cos\theta_2}e \\ \beta = \dfrac{2\pi}{\lambda}\cos(\theta_2)ne \end{cases}. \tag{3}$$

At Brewster's angle given by [19]

$$\theta_B = \arctan(n), \tag{4}$$

the reflection coefficient for the p-polarization coefficient r_{12}^p vanishes to zero, while reflection coefficient for the s-polarization is stronger than for normal incidence. The p-polarized component of the impinging wave is then fully transmitted, while the s-polarized component is partially reflected (see Fig. 2, solid lines). This induces a partial polarization of the light, and it has been used as a polarizer in the visible range since the 19th century [20]. Most importantly, there is no stray reflection at both interfaces and the wave is fully transmitted, meaning that

#146467 - $15.00 USD Received 26 Apr 2011; revised 17 Jun 2011; accepted 18 Jun 2011; published 8 Jul 2011

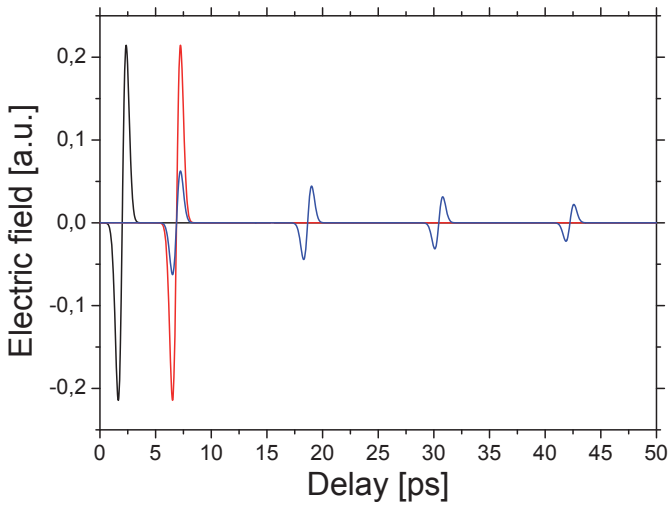

Fig. 3. Theoretical propagation of a terahertz pulse (black) through a silicon plate, for p-polarization (red) and s-polarization (blue), with a plate thickness $e = 540\mu$m and an incidence angle at Brewster's angle, for $n = 3.41$.

there is no Fabry-Pérot effect into the plate when lit at Brewster's angle. This is particularly important when dealing with THz pulses since no echoes are expected. Figure 3 illustrates the theoretical transmissions of a terahertz pulse, with respect to incident polarization, at Brewster's angle ($\theta_1 = \theta_B$). The p-polarized pulse is fully transmitted, while the s-polarized pulse exhibits many oscillations.

Finally, the light going through the plate is delayed by the additional optical path

$$\Delta t = \frac{e}{c\cos\theta_2}\left[n - \cos(\theta_1 - \theta_2)\right], \tag{5}$$

the beam undergoes a small walk-off calculated as

$$w = e\frac{\sin(\theta_1 - \theta_2)}{\cos(\theta_2)} = e\left[\sin\theta_1 - \frac{\cos^2\theta_1}{\sqrt{n^2 - \sin^2\theta_1}}\right] \tag{6}$$

and the travel d in the wafer is

$$d = \frac{ne}{\sqrt{n^2 - \sin^2\theta_1}}. \tag{7}$$

Finally, the extinction ratio is defined as

$$\rho = \frac{T_p}{T_s}. \tag{8}$$

Since a single wafer at Brewster's angle still transmits some *s*-component, relatively low extinction ratio is obtained by only one plate. In order to improve the extinction ratio, it is necessary to use a stack of wafers. Since $T_p = 1$ at Brewster's incidence,

$$\rho_k = 1/T_s^k \tag{9}$$

with k the number of wafers forming the complete polarizer. Figure 4 shows the number of required wafers to achieve a 10^2 (20 dB) extinction ratio in amplitude (or 10^4, 40dB in intensity),

#146467 - $15.00 USD Received 26 Apr 2011; revised 17 Jun 2011; accepted 18 Jun 2011; published 8 Jul 2011

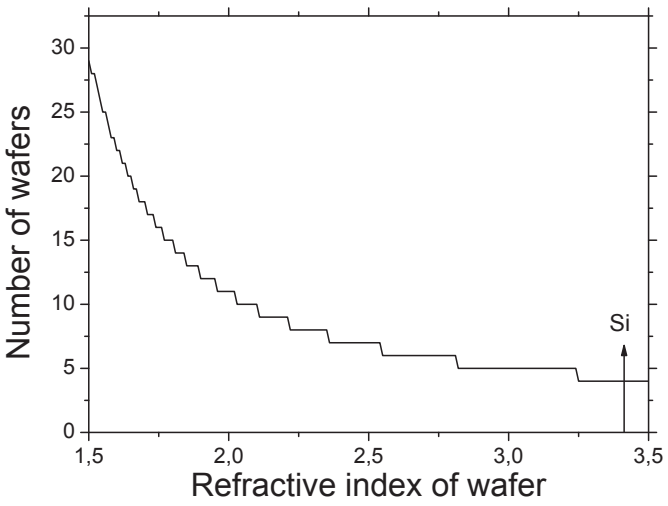

Fig. 4. Number of wafer required to get an amplitude extinction ratio of at least 10^2 (20 dB amplitude, 40 dB intensity) versus the refractive index of the wafer.

with respect to the refractive index. We observe that the number of plates strongly diminishes for high refractive index. Therefore, only four silicon plates are required to achieve the targeted extinction ratio, since $n_{Si} = 3.41$ [1]. For common THz-compliant materials with low refractive index such as polyethylene or Teflon ($n \approx 1.5$), the total number of plates would exceed 20, which make the use of a pile a plate rather difficult, since these materials exhibit non negligible absorption in the terahertz range.

Furthermore, the stacking of wafers potentially gets rise to echoes between wafers, characterized by a lateral shift Δ and time delay τ, given by

$$\Delta = \frac{h \sin 2\theta}{\cos\theta} \quad \text{and} \quad \tau = \frac{2L}{c} \quad \text{with} \quad L = \frac{h}{\cos\theta}. \tag{10}$$

Thanks to the lateral shift, these echoes can easily be canceled out by the exit aperture of the polarizer.

3. Experimental setup

To generate the THz signal, we used a classical THz-TDS setup [1], composed of a photoconductive antenna $\mathrm{Tx}_{\parallel}$ lit by a 12 fs, Femtolaser Ti:Sa laser, that generates an almost linearly polarized sub-single cycle THz pulse, centered around 1 THz, at a repetition rate of 76 MHz. The pulse is then collimated with an off-axis parabolic mirror (OAPM) onto the system under study. Then, the THz beam is split into two parts using a 3 mm-thick silicon wafer beam splitter at 45° (Si-BS, $T_p = 0.82$, $r_s = -0.65$), and both sides are focused with OAPMs. The two polarization components of the THz wave are finally detected by two orthogonal photoswitch antennas $\mathrm{Rx}_{\parallel}$ and $\mathrm{Rx}_{\perp}$, each detecting only one component of the THz wave (see Fig. 5). A main delay line τ_1 allows scanning the waveform of the pulse, while a second one τ_2 allows finely tuning the optical path between the two detecting antennas which must be equal. The gain reception antenna perpendicular to the emission antenna is calibrated so as to match with the gain of the other. The whole system is placed into a box filled with dry nitrogen to get rid of water vapor absorption ($< 1.2\%$ residual relative humidity). A mechanical chopper and lock-in detection are used to increase the signal-to-noise ratio of the system.

#146467 - $15.00 USD Received 26 Apr 2011; revised 17 Jun 2011; accepted 18 Jun 2011; published 8 Jul 2011

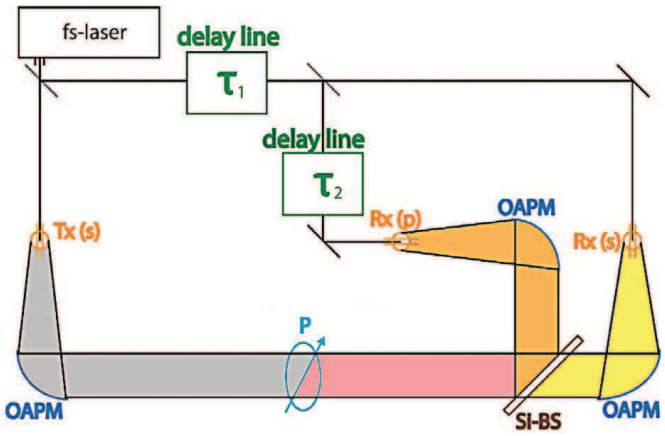

Fig. 5. Experimental setup. Tx: photoconductive emitter; OAPM: off-axis parabolic mirror; P: polarizer; Si-BS: silicon beam splitter; Rx and Rs: receivers.

4. Single wafer measurements

First, we studied the behavior of a single wafer under rotation. We used a standard industry-grade circular wafer having a diameter $D = 100\,\text{mm}$ and thickness $e = 525\,\mu\text{m} \pm 25\,\mu\text{m}$, with a constant refractive index of $n = 3.41$, leading to a Brewster's angle of $\theta_B = 73.6°$. We placed the wafer on a rotating mount and recorded the full waveform of the THz pulse for each incidence angle. This lead to two sets of measurements, for the determination of the s- and p- polarization transmission coefficients. We used only one detector (Rx($\|$)) for the measurement since the second one would detect no signal for the emitted THz pulse assumed to be linearly polarized. The aperture of the system is $A = e\cos\theta$, that is 28 mm at θ_B, what is sufficient for most THz experiment. Since we used a diaphragm smaller than the OAPM aperture, this detected signal level does not sensibly suffer from walk-off (0.45 mm for θ_B in silicon).

We can see on Fig. 6 that the main transmitted pulse amplitude for the *s*-component decreases, while it increases for the *p*-component, alongside with a decrease of the Fabry-Pérot effect, when the angle of incidence is increased all the way to Brewster's angle. There is an increasing time-delay for both polarizations due to the increased optical path. As can be seen, the experimental data (dots) match very well with theory (lines), where the reference pulse without wafer has been applied the theoretical transfer function (Eq. (3)). The measured relative transmission amplitudes also compare very well with theory, as can be seen in Fig. 2 (dots).

5. Multiple wafers polarizer measurements

Considering a linearly polarized THz electric field propagating through a perfect linear polarizer rotating around the optical axis with an angle α, the two transmitted amplitude components $E_\parallel$ and $E_\perp$ are given by

$$\begin{bmatrix} E_\parallel \\ E_\perp \end{bmatrix} = \begin{bmatrix} \cos\alpha & -\sin\alpha \\ \sin\alpha & \cos\alpha \end{bmatrix} \begin{bmatrix} 1 & 0 \\ 0 & 0 \end{bmatrix} \begin{bmatrix} \cos\alpha & \sin\alpha \\ -\sin\alpha & \cos\alpha \end{bmatrix} \begin{bmatrix} E_0 \\ 0 \end{bmatrix} = \frac{E_0}{2} \begin{bmatrix} 1+\cos(2\alpha) \\ \sin(2\alpha) \end{bmatrix} \quad (11)$$

Attentive reader will observe that the derived equation [Eq. (11)] differs from Malus' law [21], which concerns the power detected by a polarization-insensitive detector when a linear polarizer cancels out a linearly polarized light. Indeed, the amplitude $E_\perp$ is counter-intuitively

#146467 - $15.00 USD Received 26 Apr 2011; revised 17 Jun 2011; accepted 18 Jun 2011; published 8 Jul 2011

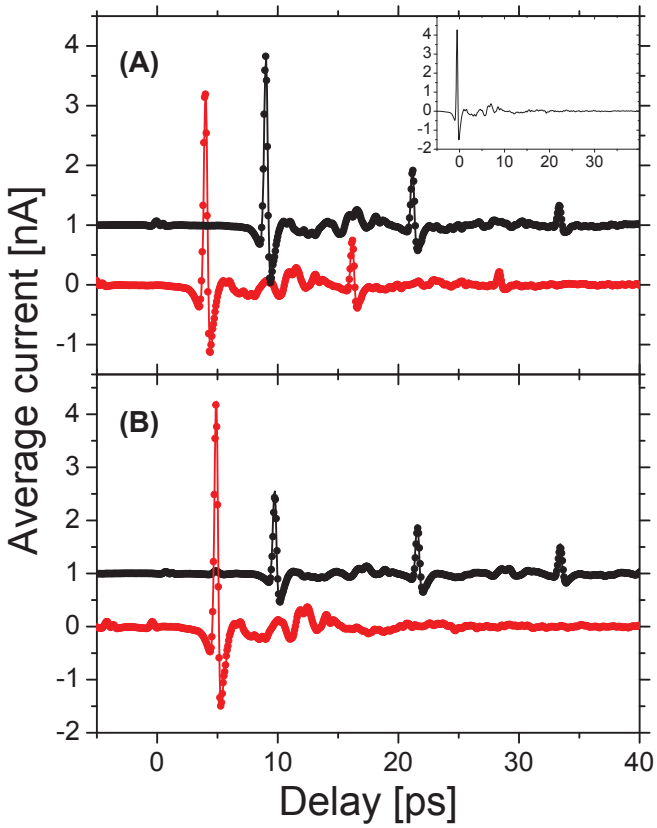

Fig. 6. Experimental terahertz waveforms of s- (black) and p- (red) polarization components after the propagation through a silicon wafer for two incidence angles of 30° (A) and Brewster's angle at 73° (B), for experimental data (dots) and theoretical calculation using Eq. (3) (lines).

dephased and allowed to be negative, *i.e.* the polarity of the THz pulse can potentially be reversed by the linear polarizer.

We now consider a more complex polarizer made from a stack of 4 silicon wafers. We used 4 mm spacing in our Brewster's polarizer (see Fig. 7). The 4 silicon wafers are mounted tightly together with spacers on a square holder, fixed perpendicularly to a motorized rotating stage. The direction of polarization is then given by the plane of the wafers. The two orthogonal electric field components of the THz pulse transmitted through the 4-wafer polarizer are shown in Fig. 8. First, we observe no distortion in the pulse traveling through the polarizer. The polarizer delays the reference pulse, but demonstrates very good transmission efficiency ($> 99\%$) for $E_{\parallel}$ (Fig. 8(A) black lines). Transmission at 90° (blue line in Fig. 8(A)) shows a crossed-polarized extinction factor of 78 (18.9 dB) in amplitude corresponding to 6×10^3 (37.8 dB) in power, and shows better results that with wire-grid polarizers [8] The expected phase inversion is also found in the orthogonal component (Fig. 8(B), green line). Details of the transmitted pulse on longer time delays are depicted in Fig. 9 for the parallel $E_{\parallel}$ and orthogonal $E_{\perp}$ components. The echo observed at a delay of about 70 ps is due to the 3 mm-thick silicon beam splitter. Inset shows an expansion of $E_{\perp}$ for clarity. Residual oscillation originates from echoes inside the silicon wafers, corresponding to a time delay $\tau \approx 12$ ps (see Eq. (10)).

#146467 - $15.00 USD Received 26 Apr 2011; revised 17 Jun 2011; accepted 18 Jun 2011; published 8 Jul 2011

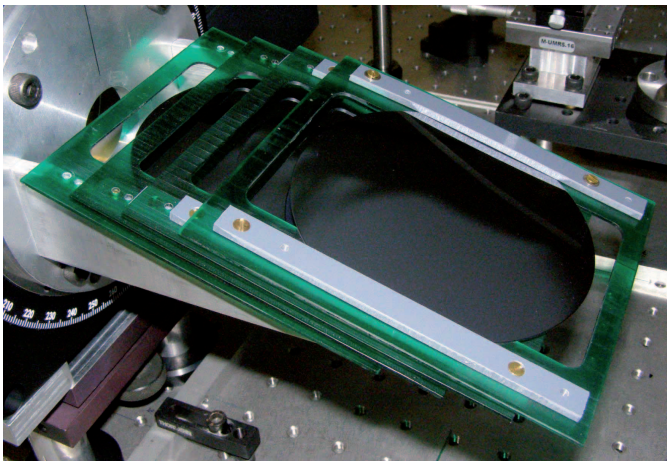

Fig. 7. Picture of the 4-wafer silicon polarizer.

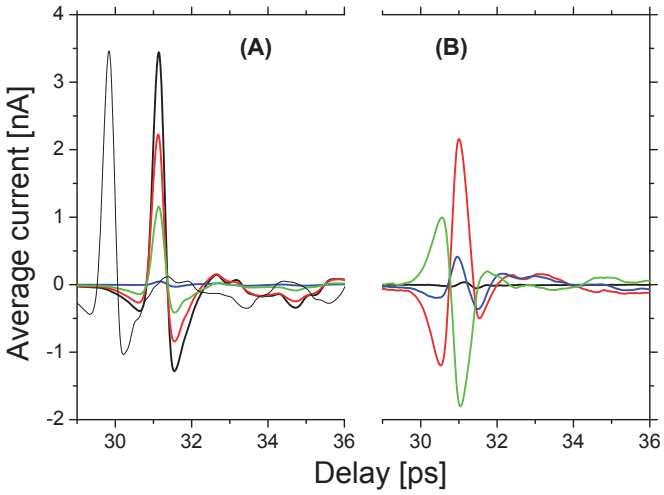

Fig. 8. Parallel (A) and orthogonal (B) components of the THz pulse after propagation through the 4-wafer silicon polarizer at several orientations. Reference pulse (thin black line) is shifted by $+20$ ps. Orientations α are 0° (thick black), 45° (red), 90° (blue) and 135° (green).

The last measurement is done by rotating the 4-wafer silicon polarizer to check the angular response. Figure 10 plots the relative amplitude maximums of the transmitted THz pulse, as a function of the relative angle α for $E_{\parallel}$ and $E_{\perp}$. It shows a very good agreement between the data (dots) and the theoretical calculations (solid lines). To avoid residual cross-polarization signal in the detectors, additional polarizers were used in both emitter and detectors. Similar results are obtained in the frequency domain using Fourier transform of the time domain data, but phase information are lost. Time domain data allow a full description of Brewster's polarizing effect.

#146467 - $15.00 USD Received 26 Apr 2011; revised 17 Jun 2011; accepted 18 Jun 2011; published 8 Jul 2011

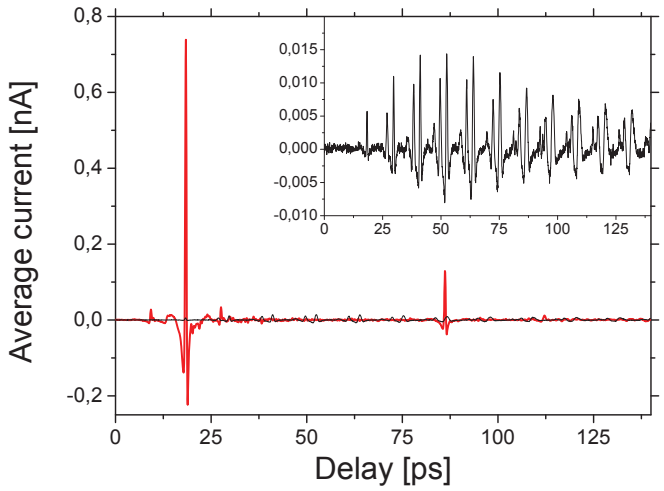

Fig. 9. Parallel $E_{\parallel}$ (black) and orthogonal $E_{\perp}$ (red) components of the THz pulse after propagation through the 4-wafer silicon polarizer. Inset is an expansion of $E_{\perp}$.

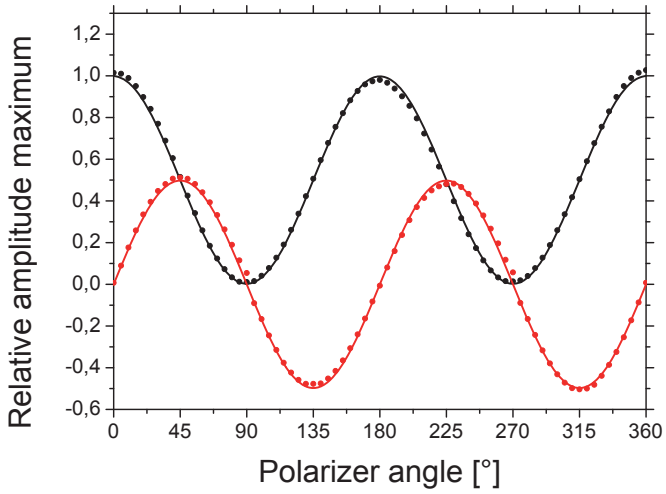

Fig. 10. Detected maximum amplitude for various angle of the 4-wafer silicon polarizer mounted on a rotation stage, for parallel $E_{\parallel}$ (black) and orthogonal $E_{\perp}$ (red) electric field components. Dots are experimental data and solid lines are theoretical calculations.

6. Conclusion

We showed that the Fresnel coefficients at dielectric interface can be very efficiently put in practice for the design of a low-cost, low insertion loss and high extinction ratio linear polarizer. Using four industrial grade silicon wafers, we obtained a power extinction ratio of more than 6×10^3, that outperforms most of the conventional wire-grid polarizer. Higher performances can easily be obtained using more silicon wafers.

#146467 - $15.00 USD Received 26 Apr 2011; revised 17 Jun 2011; accepted 18 Jun 2011; published 8 Jul 2011